Acta Cryst. (1974). A30, 265

Continuous Structure Variation and Rotating Reciprocal Lattices in the Titanium – Chromium Oxides

BY D. K. PHILP* AND L. A. BURSILL

School of Chemistry, University of Western Australia, Nedlands, 6009 Australia

(*Received* 25 *September* 1973; *accepted* 17 *October* 1973)

High-index, rutile-derived, crystallographic shear (CS) structures occupy the composition range (Ti, Cr)O_x, $1{\cdot}875 \le x \le 1{\cdot}93$. The CS plane rotates continuously from $(121)_r$ to $(132)_r$, about the $[1\bar{1}1]_r$ zone axis, producing a continuous series of intermediate CS planes with $(hkl)_r = p\,.\,(121)_r + q\,.\,(011)_r$. In the reciprocal lattice a fine net of superstructure reflexions rotates continuously relative to a coarse net of rutile subcell reflexions. Analogous reciprocal-lattice behaviour should be a general crystallographic phenomena and may appear in any system where superstructures occur. It is shown how the intermediate diffraction patterns may be indexed by deriving a single transformation matrix relating the unit cells of the high-index superstructures to that of the basic subcell.

Introduction

Ordered crystallographic shear (CS) structures M_nO_{2n-1}, $4 \le n \le 9$, with M = Ti or (Ti, Cr), were discovered by powder and single-crystal X-ray diffraction methods (Andersson & Jahnberg, 1963; Andersson, 1960). They may be formally derived from rutile by the regular action of the displacement vector $\frac{1}{2}[0\bar{1}1]_r$† across $(121)_r$ planes. Electron microscopy and diffraction techniques established the existence of ordered CS structures Ti_nO_{2n-1}, $16 \le n < 36$ with the same displacement vector acting across $(132)_r$ planes (Bursill, Hyde, Terasaki & Watanabe, 1969; Bursill & Hyde, 1970, 1971). Recent electron-diffraction work showed the existence of at least 50 structures in the intermediate composition range MO_x, $1{\cdot}875 \le x \le 1{\cdot}93$ for M = Ti and (Ti, Cr) (Bursill, Hyde & Philp, 1971; Philp & Bursill, 1974). The CS plane rotates continuously from $(132)_r$ to $(121)_r$, about the $[1\bar{1}1]_r$ zone axis, producing a continuous series of high-index intermediate CS planes with

$$(hkl)_r = p\,.\,(121)_r + q\,.\,(011)_r\,,$$

where p and q are integers.

In the reciprocal lattice a fine net of superstructure reflexions rotates continuously relative to a coarse net of rutile subcell reflexions (see Fig. 4 in Bursill *et al.*, 1971). The reflexions strong enough to be observed by X-ray diffraction are doublets and triplets centred approximately at the subcell positions. In the swinging CS plane region the X-ray powder lines show only small shifts. The existence of a large number of ordered structures with variable CS plane is therefore concealed and it could be assumed that the composition range contains only one wide-range nonstoichiometric phase. Florke & Lee (1970) assumed instead that the $(121)_r$ family continued up to $n = 17$ and blamed poor resolution for the apparently continuous line shifts.

We believe that this type of reciprocal-lattice behaviour is a general crystallographic phenomenon and will be revealed in numerous systems where superstructures occur. To detect and distinguish high-index structures it is essential that single-crystal patterns be used. These must be very carefully oriented into specific zones. Even electron-diffraction patterns (which record a much higher proportion of the allowed reflexions than do X-ray patterns) are fully extended to reveal the subtle changes that occur.

It is shown below how the intermediate diffraction patterns may be indexed by deriving a single transformation matrix relating the unit cells of the high-index structures to the rutile unit cell.

Experimental results

82 $[1\bar{1}1]_r$ zone-axis diffraction patterns were obtained in the course of a phase-analysis study of rutile plus O to 25 mol.% $CrO_{1.5}$ (Philp, 1972; Philp & Bursill, 1974). Details of the preparation methods, composition calculations and measurements of CS plane spacing (D_{sp}) and orientation ($p' = p/q$) are given in these references. D_{sp} may be measured to approximately 1% accuracy using an internal standard. The accuracy of p' varies from 1 to 6% for $p' = 1$ to 10. Four typical diffraction patterns are shown in Fig. 1. Of the 82 diffraction patterns obtained, 50 were measurably different.

Swinging CS plane structures

It is well known that the oxygen array in rutile may be idealized to h.c.p. by flattening the puckered $(100)_r$

* Present address: Defence Standards Laboratories, P.O. Box 50, Ascot Vale, 3032 Australia.

† Subscript r refers to indices based on the rutile cell or subcell.

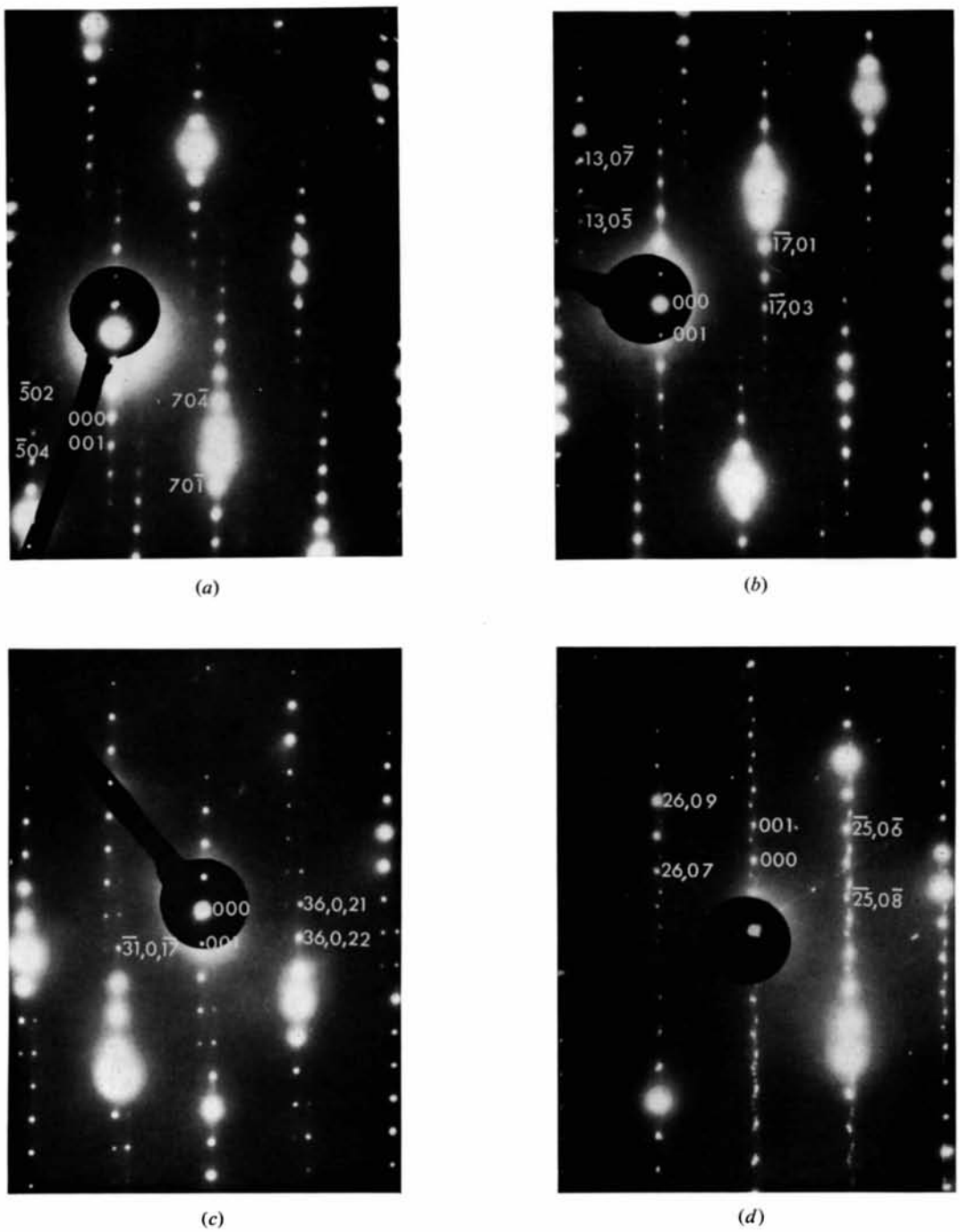

Fig. 1. Four indexed [1$\bar{1}$1], zone axis diffraction patterns. (*a*) $p=5$, $q=2$, $n=68$, origin shifted by g(003), plate number 23177. (*b*) $p=13$, $q=4$, $n=149$, plate number 23672. (*c*) $p=31$, $q=5$, $n=307$, plate number 23621. (*d*) $p=25$, $q=1$, $n=223$, origin shifted by g(002), plate number 23904.

[*To face p.* 265

planes. The metal atoms occupy half the octahedral interstices, so as to give strings of edge-shared TiO_6 octahedra, joined by corner-sharing. Fig. 2(*a*) shows an idealized octahedral drawing of rutile projected along $[100]_r$. The idealized oxygen array is common to all the CS structures because the displacement vector, $\frac{1}{2}[0\bar{1}1]_r$, lies in the $(100)_r$ plane and is exactly an oxygen–oxygen vector. It is therefore convenient to draw only the metal-atom positions. There are two layers per repeat normal to $(100)_r$. They have identical metal arrays and adjacent layers are displaced by $\frac{1}{2}[1\bar{1}1]_r$ so that we need draw only one $(100)_r$ metal-atom layer to obtain a simplified representation of the structure. This is compared with the octahedral drawing in Fig. 2(*b*).

Drawings of such metal-atom layers intersected by $(121)_r$ and $(132)_r$ CS planes, and an $(011)_r$ anti-phase boundary (APB) are shown in Fig. 3. Along the trace of the $(132)_r$ CS plane $(121)_r$ and $(011)_r$ steps alternate. We call these basic structural elements C and A type steps [Fig. 4(*a*), (*b*)]. In three dimensions these become $[1\bar{1}1]_r$ chains of corundum-like and α-PbO_2 type structures (with edge- and face-sharing octahedra or corner- and edge-sharing octahedra respectively) [Fig. 4(*c*), (*d*)]. All three faults are contained in the $[1\bar{1}1]_r$ zone so that

$$(132)_r\tfrac{1}{2}[0\bar{1}1]_r=(121)_r\tfrac{1}{2}[0\bar{1}1]_r+(011)_r\tfrac{1}{2}[0\bar{1}1]_r\,.$$

In general, leaving out the common vector,

$$(hkl)_r=p(121)_r+q(011)_r\,.$$

Along unit length of CS plane trace there are p C steps and q A steps. Within the CS plane there are p corundum and q α-PbO_2 chains per repeat.

The production of an ordered CS structure effectively involves the elimination of p out of every $2n$ oxygen-only $(hkl)_r$ planes (see Fig. 21 of Bursill & Hyde, 1972). The stoichiometry is thus M_nO_{2n-p}. Alternatively the high-index structures, like the CS planes, may be regarded as intergrowths of $(121)_r$ and $(011)_r$ CS elements. Thus

$$M_nO_{2n-p}=p\,.\,M_{n_1}O_{2n_1-1}+q\,.\,M_{n_2}O_{2n_2}\,,$$

where

$$n=n_1p+n_2q\,.$$

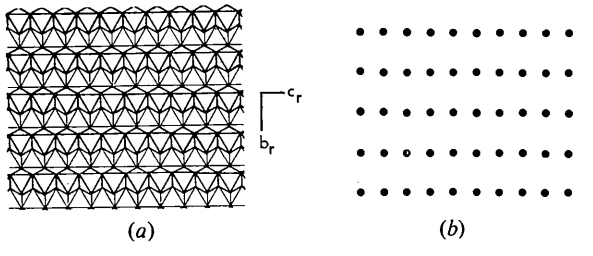

Fig. 2. (*a*) Idealized rutile structure, $(100)_r$ plane; $z=0$ and $z=\frac{1}{2}$ layers. (*b*) Dot diagram of rutile structure, showing only metal atoms at $z=0$.

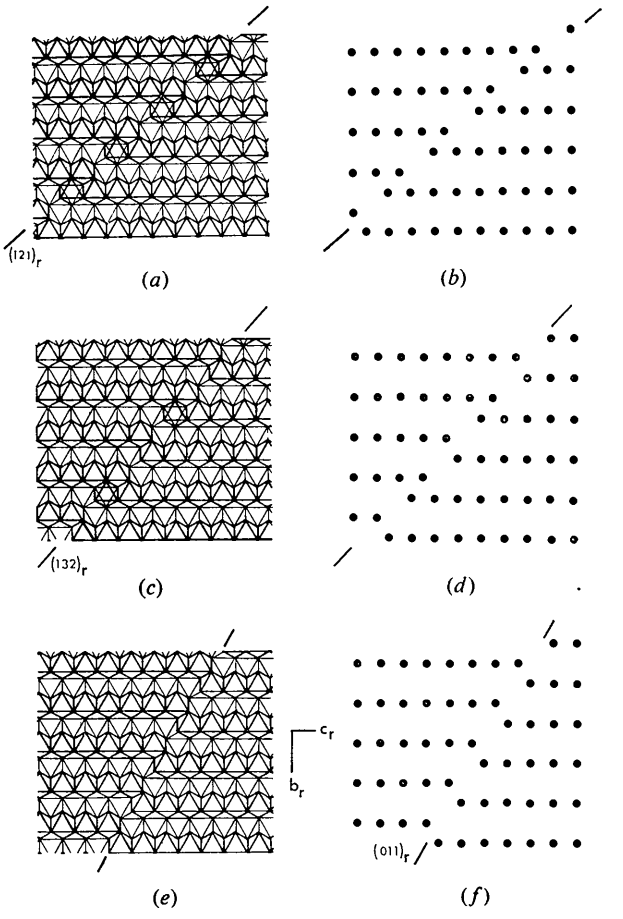

Fig. 3. (*a*) Idealized octahedral diagram of the trace of a (121) CS plane on $(100)_r$. (*b*) Dot representation of (*a*). (*c*) Octahedral drawing of trace of $(132)_r$ CS plane. (*d*) Dot representation of (*c*). (*e*) Octahedral drawing of trace of $(011)_r$ anti-phase boundary. (*f*) Dot representation of (*e*).

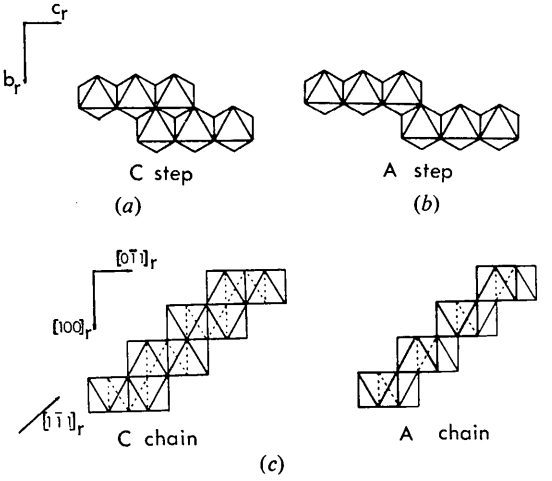

Fig. 4. (*a*) C-step structural unit in $(100)_r$ plane. (*b*) A-step structural unit in $(100)_r$ plane. (*c*) C-type corundum-like $[1\bar{1}1]_r$ chain of edge- and face-shared octahedra. (*d*) A-type α-PbO_2-like $[1\bar{1}1]_r$ chain of edge- and corner-shared octahedra.

For instance $n=25$ $(253)_r$ ($p=2$, $q=1$) may be resolved as

$$2M_9O_{17}+M_7O_{14} \quad (n_1=9,\ n_2=7) \quad \text{[Fig. 5(a)]}$$

or as

$$2M_{10}O_{19}+M_5O_{10} \quad (n_1=10,\ n_2=5) \quad \text{[Fig. 5(b)]},\ \textit{etc.}$$

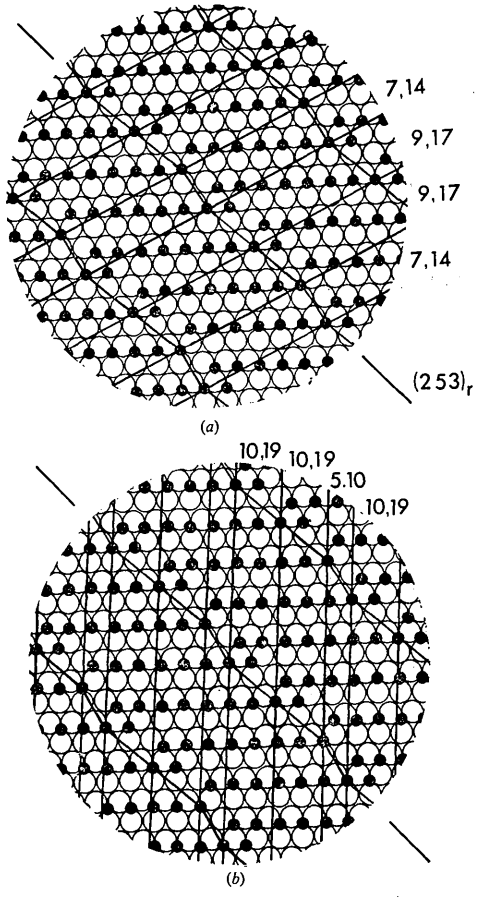

Fig. 5. Resolution of $(253)_r$ CS structure into ordered intergrowths of $(121)_r$ and $(011)_r$ shear structures. (*a*) $M_{25}O_{48}$ $(253)_r=2M_9O_{17}$ $(121)_r+M_7O_{14}$ $(011)_r$. (*b*) $M_{25}O_{48}$ $(253)_r=2M_{10}O_{19}$ $(121)_r+M_5O_{10}$ $(011)_r$.

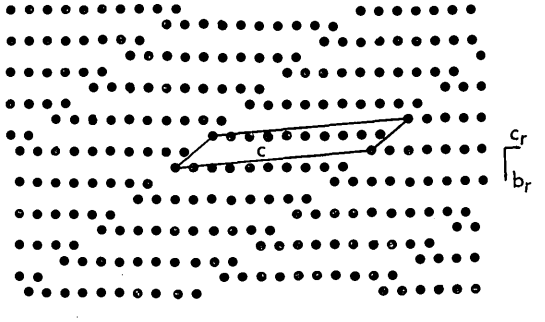

Fig. 6. $n=10$ $(121)_r$ CS structure.

Matrix relations between unit cells

a and **b** axes are chosen so that $\mathbf{a}\times\mathbf{b}$ is normal to the CS plane, and thus defines its orientation. A convenient choice is

$$\mathbf{a}=p\mathbf{a}_r+q\mathbf{b}_r-(p+q)\mathbf{c}_r\,,$$

$$\mathbf{b}=-\mathbf{a}_r+\mathbf{b}_r-\mathbf{c}_r\,.$$

c is chosen in the $(100)_r$ plane (*i.e.* in the plane of the drawings); it defines the CS plane spacing(s).

(*a*) $q=0$. In $(121)_r$ structures all steps are C type. There is only one step per repeat along the CS plane trace, and there are n metal atoms in each $\mathbf{c}_r$ axis string of edge-shared octahedra. Fig. 6 shows $n=10$. The **c** axis is simply

$$\mathbf{c}=-\tfrac{1}{2}\mathbf{b}_r+(n+\tfrac{1}{2})\mathbf{c}_r\,.$$

(*b*) $q=1$. Fig. 7 shows five adjacent members of the $(495)_r$ family: $p=4$, $n=41$ to 45. For $n=45$ all strings contain 9 metal atoms but, as n decreases, the A steps on the right-hand CS plane move down relative to those on the left-hand CS plane. At each change in n one additional row loses a metal atom and the string lengths change from 9, 9, 9, 9, 9, in $n=45$, to 8, 9, 9, 9, 9 in $n=44,\ldots,$ to 8, 8, 8, 8, 8 in $n=40$. Clearly strings are all of the same length ($=k$) if n is a multiple of $(p+q)$, but not otherwise. k is the smallest integer greater than or equal to $n/(p+q)$ and may be written

$$k=n/(p+q)+1-|n/(p+q)|_1\,.$$

The parameter r is introduced to simplify the expression for **c**. When all the strings have the same length we take $r=0$; thus $r=0$, 1, 2, 3, 4 and 0 for $n=$ 45, 44, 43, 42, 41 and 40 respectively (see Fig. 7). For $q=1$ *only*, r of the strings have $(k-1)$ metal atoms and

$$r=k(p+q)-n\,.$$

The **c** axis is now

$$\mathbf{c}=(r-\tfrac{1}{2})\mathbf{b}_r+(k+\tfrac{1}{2}-2r)\mathbf{c}_r\,.$$

(*c*) $q\geq 2$.* Consider, for example, the $(8,19,11)_r$ CS family ($p=8$, $q=3$). Fig. 8 shows $99\geq n\geq 89$, r runs from 0 to 10. The number of strings which have $(k-1)$ metal atoms is now $|rq|_{p+q}$, which is the smallest positive number less than $(p+q)$ remaining after repeatedly subtracting $(p+q)$ from (rq).

Thus

$$|rq|_{(p+q)}=k(p+q)-n\,.$$

For example, for $n=91$, $91=99-|3r|_{11}$, *i.e.* $|3r|_{11}=8$ and therefore $3r=30$ and $r=10$.

* In the following discussion it is assumed $p>q$. However the resultant matrix applies, without modification, for $q>p$. In the latter case it is more convenient to choose the origin at a C rather than an A step.

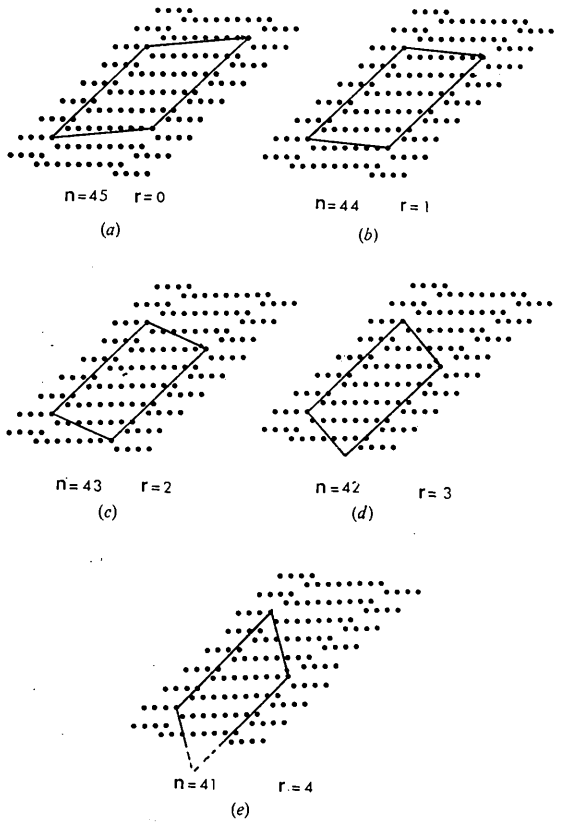

Fig. 7. Five members of the (495)$_r$ CS family: (*a*) $n=45$, $r=0$, (*b*) $n=44$, $r=1$, (*c*) $n=43$, $r=2$, (*d*) $n=42$, $r=3$, (*e*) $n=41$, $r=4$.

Three subsets of structures may be distinguished for $0\le r\le 10$. The **c** axes are

(1)
$$\begin{aligned}
\mathbf{c}_{99} &= -\tfrac{1}{2}\mathbf{b}_r + 9\tfrac{1}{2}\mathbf{c}_r, & r=0;\\
\mathbf{c}_{96} &= \tfrac{1}{2}\mathbf{b}_r + 7\tfrac{1}{2}\mathbf{c}_r, & r=1;\\
\mathbf{c}_{93} &= 1\tfrac{1}{2}\mathbf{b}_r + 5\tfrac{1}{2}\mathbf{c}_r, & r=2;\\
\mathbf{c}_{90} &= 2\tfrac{1}{2}\mathbf{b}_r + 3\tfrac{1}{2}\mathbf{c}_r, & r=3;
\end{aligned}$$

(2)
$$\begin{aligned}
\mathbf{c}_{98} &= 3\tfrac{1}{2}\mathbf{b}_r + 2\tfrac{1}{2}\mathbf{c}_r, & r=4;\\
\mathbf{c}_{95} &= 4\tfrac{1}{2}\mathbf{b}_r + \tfrac{1}{2}\mathbf{c}_r, & r=5;\\
\mathbf{c}_{92} &= 5\tfrac{1}{2}\mathbf{b}_r - 1\tfrac{1}{2}\mathbf{c}_r, & r=6;\\
\mathbf{c}_{89} &= 6\tfrac{1}{2}\mathbf{b}_r - 3\tfrac{1}{2}\mathbf{c}_r, & r=7;
\end{aligned}$$

(3)
$$\begin{aligned}
\mathbf{c}_{97} &= 7\tfrac{1}{2}\mathbf{b}_r - 4\tfrac{1}{2}\mathbf{c}_r, & r=8;\\
\mathbf{c}_{94} &= 8\tfrac{1}{2}\mathbf{b}_r - 6\tfrac{1}{2}\mathbf{c}_r, & r=9;\\
\mathbf{c}_{91} &= 9\tfrac{1}{2}\mathbf{b}_r - 8\tfrac{1}{2}\mathbf{c}_r, & r=10.
\end{aligned}$$

Decreasing r by 1 moves all the A steps on the right-hand CS plane down relative to those on the left-hand CS plane (see Fig. 8), thus changing n by 3 (q in general). Three (q) subsets arise because, relative to the left-hand CS plane, an A step on the right-hand CS plane [circled in Fig. 8(*a*),(*e*),(*i*)] may initiate one of three sequences,

... A C C C A C C C A C C A ...
or ... A C C C A C C A C C C A ...
... A C C A C C C C A C C C A ....

Changing r by 1 moves all 3 A steps per repeat, and since n changes by 1 each time 1 A step moves then changing r by 1 changes n by 3. Fig. 8 shows that $n=99$ and 98 ($r=0$ and 4 respectively) differ by the jump of only 1 A step, although the **c** axes differ dramatically.

In order to write down an expression for **c** in the most general case it is convenient to introduce a further parameter s. We take $s=0$ for $q=1$ (and for $q=0$) but take integral values $0\le s\le q-1$ for $q\ge 2$, where s is given by

$$s=|k(p+q)-n|_q\,.$$

Thus, for
$$\begin{aligned}
0\le r\le 3 \quad & s=0,\\
4\le r\le 7 \quad & s=1,\\
8\le r\le 10 \quad & s=2.
\end{aligned}$$

We may then write

$$\mathbf{c}=(r-\tfrac{1}{2})\mathbf{b}_r+(k+\tfrac{1}{2}-2r+s)\mathbf{c}_r\,.$$

The resultant complete matrix is

Rutile

$$\mathrm{M}_n\mathrm{O}_{2n-p}\begin{pmatrix} \underline{p} & q & \overline{p+q} \\ \overline{1} & 1 & \overline{1} \\ 0 & r-\tfrac{1}{2} & k+\tfrac{1}{2}-2r+s \end{pmatrix}$$

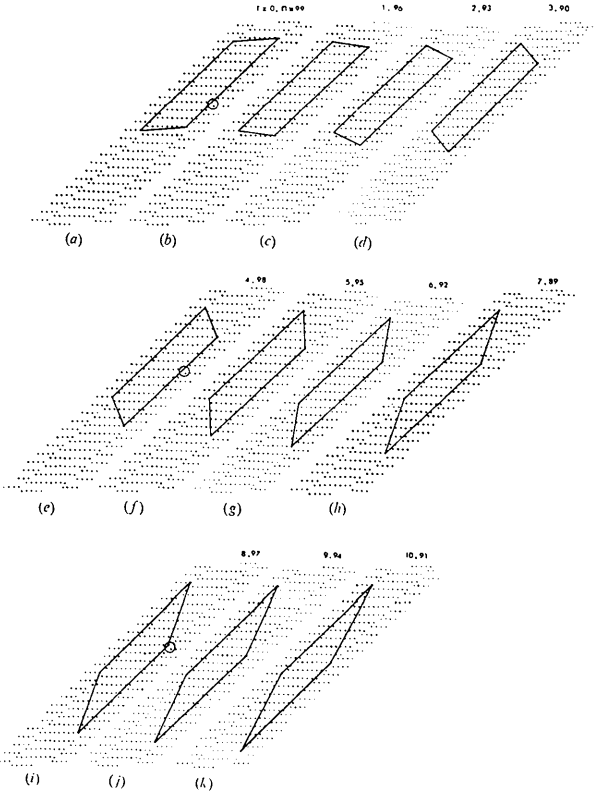

Fig. 8. Eleven members of the (8, 19, 11)$_r$ CS family, $p=8$, $q=3$: (*a*) $n=99$, $r=0$, $s=0$, (*b*) $n=96$, $r=1$, $s=0$, (*c*) $n=93$, $r=2$, $s=0$, (*d*) $n=90$, $r=3$, $s=0$, (*e*) $n=98$, $r=4$, $s=1$, (*f*) $n=95$, $r=5$, $s=1$, (*g*) $n=92$, $r=6$, $s=1$, (*h*) $n=89$, $r=7$, $s=1$, (*i*) $n=97$, $r=8$, $s=2$, (*j*) $n=94$, $r=9$, $s=2$, (*k*) $n=91$, $r=10$, $s=2$.

where $k=n/(p+q)+1-|n/(p+q)|_1$,

$|rq|_{(p+q)}=k(p+q)-n$,

$s=|k(p+q)-n|_q$.

Solving for $\mathbf{a}_r$, $\mathbf{b}_r$ and $\mathbf{c}_r$ in the above matrix yields the inverse matrix

$$\begin{array}{c} \\ \text{Rutile} \\ \frac{1}{\Delta} \end{array} \begin{array}{c} \mathrm{M_nO_{2n-p}} \\ \begin{pmatrix} k-r+s & r(q-p)+p/2-q(k+s) & p \\ k+\frac{1}{2}-2r+s & p(k+\frac{1}{2}-2r+s) & 2p+q \\ -\frac{1}{2}(2r-1) & -p(2r-1)/2 & p+q \end{pmatrix} \end{array}$$

where $\Delta=(p+q)k-p/2-rq+s(p+q)$.

The relationships of this general matrix to those used previously for $(121)_r$ and $(132)_r$ families are given in the Appendix.

Unit cells for any values of p q and n are readily obtained using a computer program. In individual cases reduced cells with shorter **c** axes and angles closer to 90° may be obtained. Here it is better to use one general matrix to emphasize the overall relations. If one family is stabilized over a range in composition, separate groups of unit cells such as those used for $(121)_r$ and $(132)_r$ families may be preferred (see Appendix). The unit cells may easily be verified by building a $(100)_r$ layer using ball models. The **c** axes and cell contents may then be checked by outlining the unit cell with cotton thread and pins.

Some limitations of the above structural model

It has been assumed that p and q are coprime. A $(132)_r$ CS plane could conceivably have $p=q=N$. If $N=2$ the sequence ... C C A A C C A A ... occurs. [Note that $(132)_r$ and $(264)_r$ are parallel.] This would double the repeat distance along the CS plane. No evidence for this has been found on any of the diffraction patterns.

For $q\geq 2$ (and assuming $p>q$ here) a new possibility arises. Even for p and q coprime there will be $(p+q-1)!/[p!(q-1)!]$ possible sequences for the p C and q A steps per repeat distance along the CS plane. All of these have the same CS plane $(hkl)_r$. They may be interconverted by fixing the A step at the beginning of the sequence and rearranging the remaining $(p+q-1)$ steps by simple diffusive hops (Fig. 9). If identical hops occur in *each* unit cell then the unit-cell dimensions and stoichiometry remain unaltered. Thus, for each (n,p,q) set the above matrix gives one unit cell for which there are $(p+q-1)!/[p!(q-1)!]$ possible structures. These cannot be distinguished by their reciprocal-lattice geometry. Electron-diffraction intensity calculations are not sufficiently accurate to allow the possibilities to be distinguished by measuring spot intensities. The real structure may be a statistical assemblage of the various possible structures. The sharpness of the diffraction patterns, and the absence of diffuse scattering, suggests either a random mixture or else that one sequence is very well ordered.

In principle, parallel intergrowths of two adjacent n values in the proportions Pn_1+Qn_2 allows the composition range x_1 to x_2 to be traversed continuously. However the difference in D_{sp} for adjacent n values of high-index structures is of the same order as the accuracy of measuring D_{sp} (*e.g.* for $p'=4{\cdot}5$, $D_{sp}=1{\cdot}48$

Table 1. *CS structure indices derived from rutile indices*

$(hkl)_r$	(hkl) *CS* structure
$(110)_r$*	$[(p+q), 0, \frac{1}{2}(2r-1)]$
$(1\bar{1}0)_r$*	$[(p-q), -2, -\frac{1}{2}(2r-1)]$
$(011)_r$†	$[-p, 0, (k-r+s)]$
$(01\bar{1})_r$†	$[(p+2q), 2, (-k+3r-1-s)]$
$(101)_r$*	$[-q, -2, (k+\frac{1}{2}-2r+s)]$
$(10\bar{1})_r$*	$[(2p+q), 0, -(k+\frac{1}{2}-2r+s)]$

* Rutile reciprocal-lattice point falls between two CS structure reciprocal lattice points.

† Coincidence of rutile reciprocal-lattice point with CS structure (hkl) reciprocal-lattice point.

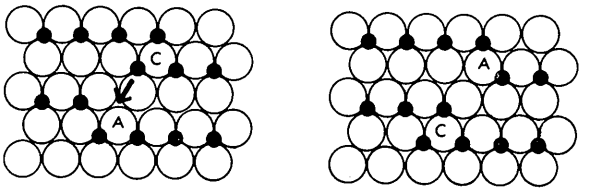

Fig. 9. Metal-atom jump required to interconvert adjacent C- and A-type steps.

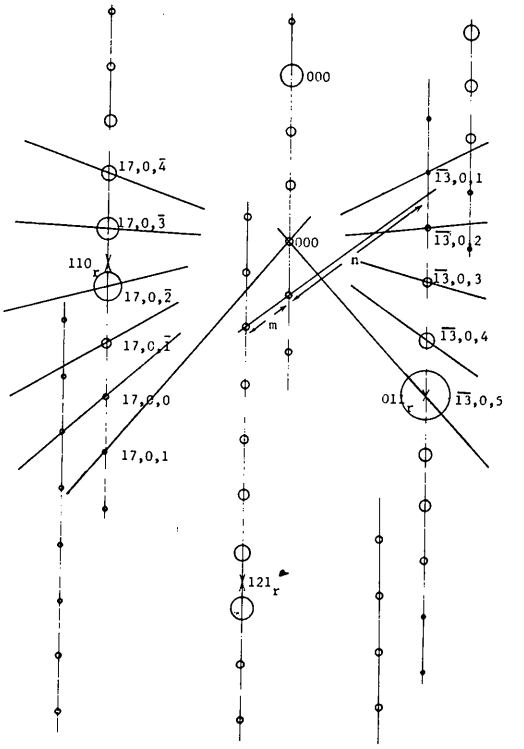

Fig. 10. Schematic drawing of a $[1\bar{1}1]_r$ zone-axis diffraction pattern, indicating the distances and angles measured and the assigned indices.

nm, $n=50$ and 51 $\Delta(D_{sp})=0{\cdot}03$ nm) so that such parallel intergrowths were not detectable in this study.

Indexing the diffraction patterns

Using a small range of p, q and n values [selected so that p/q agreed with the measured p', and n agreed with the measured $D_{sp}=(n-p/2)d_{hkl}$] a variety of suitable unit cells were generated from the above matrix by computer; and the best one selected by fitting measured and calculated d spacings and interplanar angles. (To achieve optimum sensitivity, angles close to 90° were selected.) The most intense spots were indexed by direct transformation from the readily assigned rutile indices of the $[1\bar{1}1]_r$ zone diffraction patterns (*c.f.* Table 1). (These are [010] zones for all the CS structures.)

The most readily measured angles are those be-

Table 2. *Comparison of measured and calculated data for diffraction patterns*

23177: $p=5$, $q=2$, $n=68$, $k=10$, $r=1$, $s=0$; $a=3{\cdot}260$ nm, $b=0{\cdot}7138$ nm, $c=2{\cdot}525$ nm, $\alpha=110{\cdot}74°$, $\beta=127{\cdot}83°$, $\gamma=90{\cdot}51°$.
23621: $p=31$, $q=5$, $n=307$, $k=9$, $r=25$, $s=3$; $a=17{\cdot}930$ nm, $b=0{\cdot}7138$ nm, $c=15{\cdot}802$ nm, $\alpha=41{\cdot}47°$, $\beta=59{\cdot}46°$, $\gamma=100{\cdot}52°$.

Plate number	H	K	L	Angle $\widehat{(HKL)(001)}$ (°) Meas.	Calc.	d (nm) Meas.	Calc.
23177	0	0	1	—	—	1·770	1·7756
	−5	0	3	77·6	77·95	0·624	0·6310
	−5	0	2	99·2	98·53	0·630	0·6381
	−5	0	1	117·7	117·17	0·562	0·5740
	7	0	−2	71·2	70·33	0·431	0·4339
	7	0	−3	85·9	84·40	0·456	0·4486
	7	0	−4	100·5	99·18	0·448	0·4549
23621	0	0	1	—	—	1·448	1·4470
	−31	0	−17	64·6	64·23	0·517	0·5121
	−31	0	−18	84·5	84·87	0·569	0·5664
	−31	0	−19	107·0	106·87	0·548	0·5442
	36	0	22	76·1	74·29	0·479	0·4714
	36	0	21	95·0	93·26	0·491	0·4889
	36	0	20	113·0	111·57	0·453	0·4554

Table 3. *Shift of d_{HKL} value and corresponding angle $\widehat{(HKL)}$ (001) for varying p', at constant D_{sp}*

Structure parameters.

p'	p	q	n	k	r	s	HKL	d_{HKL}	$\widehat{(HKL)}$ (001)
2·142	15	7	220	10	0	0	$\bar{1}\bar{5}$ 0 3	0·6667 nm	91·428°
2·167	13	6	190	10	0	0	$\bar{1}\bar{3}$ 0 3	0·6649	91·642
2·200	11	5	161	11	3	0	$\bar{1}\bar{1}$ 0 1	0·6628	91·013
2·250	9	4	131	11	3	0	$\bar{9}$ 0 1	0·6595	91·232
2·333	7	3	101	11	3	0	$\bar{7}$ 0 1	0·6542	91·576
2·444	22	9	314	11	3	0	$\bar{2}\bar{2}$ 0 1	0·6477	92·003
2·500	5	2	71	11	3	0	$\bar{5}$ 0 2	0·6449	88·252

Table 4. *Shift of d_{HKL} values and corresponding angles $\widehat{(HKL)}$ (001) for constant p' ($p=17$, $q=8$) and varying D_{sp}*

Three structures are compared

Structure (1): $n=256$, $D_{sp}=1{\cdot}906$ nm, $k=11$, $r=18$, $s=5$;
$a=11{\cdot}366$, $b=0{\cdot}7138$, $c=9{\cdot}894$ nm;
$\alpha=40{\cdot}14$, $\beta=50{\cdot}06$, $\gamma=87{\cdot}96°$.
Structure (2): $n=257$, $D_{sp}=1{\cdot}913$ nm, $k=11$, $r=21$, $s=6$;
$a=11{\cdot}366$, $b=0{\cdot}7138$, $c=11{\cdot}883$ nm;
$\alpha=40{\cdot}29$, $\beta=49{\cdot}23$, $\gamma=87{\cdot}96°$.
Structure (3): $n=258$, $D_{sp}=1{\cdot}921$ nm, $k=11$, $r=24$, $s=7$;
$a=11{\cdot}366$, $b=0{\cdot}7138$, $c=13{\cdot}881$ nm;
$\alpha=40{\cdot}45$, $\beta=48{\cdot}66$, $\gamma=87{\cdot}96°$.

HKL (1)	HKL (2)	HKL (3)	d_{HKL} (nm) (1)	(2)	(3)	$\widehat{(HKL)}(001)$ (°) (1)	(2)	(3)
$\bar{1}\bar{7}$ 0 $\bar{9}$	$\bar{1}\bar{7}$ 0 $\bar{1}\bar{1}$	$\bar{1}\bar{7}$ 0 $\bar{1}\bar{3}$	0·6676	0·6674	0·6670	87·77	87·20	86·64
$\bar{1}\bar{7}$ 0 $\bar{1}\bar{0}$	$\bar{1}\bar{7}$ 0 $\bar{1}\bar{2}$	$\bar{1}\bar{7}$ 0 $\bar{1}\bar{4}$	0·6379	0·6399	0·6418	107·31	106·73	106·14
25 0 15	25 0 18	25 0 21	0·4244	0·4241	0·4238	69·10	68·98	68·86
25 0 13	25 0 16	25 0 19	0·4523	0·4525	0·4527	95·43	95·19	94·94

tween 001 and $h0l$, using the $\bar{h}01$ and $h00$ rows through 011_r and 110_r (Fig. 10). The $d_{\bar{h}0l}$ values were calculated using the camera constant based on d_{011r}, which is accurate to 1% (see Philp & Bursill, 1974). To enable sufficient angles to be measured it was in many cases necessary to transpose the origin by a reciprocal lattice vector $\mathbf{g}(00l)$, $l \leq +5$. Four indexed diffraction patterns are given in Fig. 1. A comparison of measured and calculated angles and d values for two patterns is given in Table 2.

The small differences between structures are highlighted by comparing calculated d spacings and angle sizes when either p' is varied at constant D_{sp} or D_{sp} is varied at constant p'. Tables 3 and 4 exemplify this. More extended data than those given in Table 3 show that, at best, only the ends of the range $2{\cdot}143 \leq p' \leq 2{\cdot}500$ could be distinguished. Similarly, p' having been selected, the accuracy of the D_{sp} values is only sufficient to determine n to about ± 1%; *i.e.* n can only be uniquely determined if it is less than about 50.

Conclusion

We have shown that it is possible to derive unit cells which give a very good fit to the observed patterns. However, the experimental measurements are not sufficiently accurate to allow n, p and q to be determined uniquely. A list of n, p and q values for the 82 measured patterns is given elsewhere (Philp, 1972). Having assigned n, p and q we are still left with the problem of deducing the real sequence of C and A steps along the CS planes. $(p+q-1)!/[p!(q-1)!]$ ordered sequencs are possible for each set of (p, q) values. The results of a high-resolution lattice-image study attempting to reveal C and A steps and thereby study fluctuations in orientation and spacing of the CS planes will be given elsewhere (Bursill, to be published).

Commonwealth Postgraduate and Public Service Board awards to D.K.P. are gratefully acknowledged. The work was supported by the Australian Research Grants Committee and the United States Air Force Office of Scientific Research, Grant No. AFOSR-69-1806. We wish to thank Dr B. G. Hyde for his support and critical comments on the manuscript. We are also indebted to Dr L. N. D. Lucas and Mr M. K. Holmes for facilities provided at the Electron Microscope Centre of this University.

APPENDIX

Relation between the general matrix and those used previously for $(121)_r$ and $(132)_r$ structures

For the $(121)_r$ structures the direct matrix is

$$\begin{array}{c} \\ M_nO_{2n-1} \end{array} \begin{array}{c} \text{Rutile} \\ \begin{pmatrix} 1 & 0 & \bar{1} \\ \bar{1} & 1 & \bar{1} \\ 0 & -\frac{1}{2} & n+\frac{1}{2} \end{pmatrix} \end{array}$$

and the inverse matrix is

$$\begin{array}{c} \\ \text{Rutile} \end{array} \begin{array}{c} M_nO_{2n-1} \\ \frac{1}{\Delta} \begin{pmatrix} n & \frac{1}{2} & 1 \\ (n+\frac{1}{2}) & (n+\frac{1}{2}) & 2 \\ \frac{1}{2} & \frac{1}{2} & 1 \end{pmatrix} \end{array}$$

$$\Delta = n - \tfrac{1}{2}.$$

Allowing for the use of left-handed axes and a CS plane of $(1\bar{2}1)_r$ instead of $(121)_r$ by Andersson & Jahnberg, their cells are related to those in this work in the following way.

For n odd:

$$\begin{pmatrix} \mathbf{a} \\ \mathbf{b} \\ \mathbf{c} \end{pmatrix} = \begin{pmatrix} 1 & 0 & 0 \\ 0 & 1 & 0 \\ 2-n & \frac{1-n}{2} & 1 \end{pmatrix} \begin{pmatrix} \mathbf{a} \\ \mathbf{b} \\ \mathbf{c} \end{pmatrix}$$

This work. Andersson and Jahnberg.

For n even:

$$\begin{pmatrix} \mathbf{a} \\ \mathbf{b} \\ \mathbf{c} \end{pmatrix} = \begin{pmatrix} 1 & 0 & 0 \\ 0 & 1 & 0 \\ 2-n & \frac{1-n}{2} & \frac{1}{2} \end{pmatrix} \begin{pmatrix} \mathbf{a} \\ \mathbf{b} \\ \mathbf{c} \end{pmatrix}$$

This work. Andersson and Jahnberg.

In the case of the $(132)_r$ CS structures the general matrices reduce to

$$\begin{array}{c} \\ M_nO_{2n-1} \end{array} \begin{array}{c} \text{Rutile} \\ \begin{pmatrix} 1 & 1 & \bar{2} \\ \bar{1} & 1 & \bar{1} \\ 0 & \frac{1}{2}(2r-1) & (k+\frac{1}{2}-2r) \end{pmatrix} \end{array}$$

and

$$\begin{array}{c} \\ \text{Rutile} \end{array} \begin{array}{c} M_nO_{2n-1} \\ \frac{1}{\Delta} \begin{pmatrix} k-r & \frac{1}{2}-k & 1 \\ k+\frac{1}{2}-2r & k+\frac{1}{2}-2r & 3 \\ -\frac{1}{2}(2r-1) & -(2r-1)/2 & 2 \end{pmatrix} \end{array}$$

$$\Delta = 2k - \tfrac{1}{2} - r$$

where $n = 2k - r$, *i.e.* $r = 0$, n even; $r = 1$, n odd.

The cells proposed using the above matrix and those of Bursill & Hyde (1971) are related to follows, allowing for CS plane $(132)_r$ instead of $(1\bar{3}2)_r$.

For n odd:

$$\begin{pmatrix} \mathbf{a} \\ \mathbf{b} \\ \mathbf{c} \end{pmatrix} = \begin{pmatrix} 1 & 0 & 0 \\ 0 & \bar{1} & 0 \\ 1 & \bar{1} & 1 \end{pmatrix} \begin{pmatrix} \mathbf{a} \\ \mathbf{b} \\ \mathbf{c} \end{pmatrix}$$

This work. Bursill and Hyde.

For n even:

$$\begin{pmatrix} \mathbf{a} \\ \mathbf{b} \\ \mathbf{c} \end{pmatrix} = \begin{pmatrix} 1 & \bar{1} & 0 \\ 0 & \bar{1} & 0 \\ \bar{2} & \bar{3} & 1 \end{pmatrix} \begin{pmatrix} \mathbf{a} \\ \mathbf{b} \\ \mathbf{c} \end{pmatrix}$$

This work. Bursill and Hyde.

References

ANDERSSON, S. & JAHNBERG, L. (1963). *Ark. Kem.* **21**, 413–426.
ANDERSSON, S. (1960). *Acta Chem. Scand.* **14**, 1161–1172.
BURSILL, L. A. & HYDE, B. G. (1970). *Proc. Roy. Soc.* A**320**, 147–160.
BURSILL, L. A. & HYDE, B. G. (1971). *Acta Cryst.* B**27**, 210–215.
BURSILL, L. A. & HYDE, B. G. (1972). *Prog. Solid State Chem.* **7**, 177–268.
BURSILL, L. A., HYDE, B. G. & PHILP, D. K. (1971). *Phil. Mag.* **23**, 1501–1513.
BURSILL, L. A., HYDE, B. G., TERASAKI, O. & WATANABE, D. (1969). *Phil. Mag.* **20**, 347–359.
FLORKE, O. W. & LEE, C. W. (1970). *J. Solid State Chem.* **1**, 445–453.
PHILP, D. K. (1972). Ph. D. Thesis, Univ. of Western Australia.
PHILP, D. K. & BURSILL, L. A. (1974). Submitted to *J. Solid State Chem.*

Acta Cryst. (1974). A**30**, 272

A Method of Orienting Hexagonal Crystal Surfaces from Surface Trace Observations

BY H. S. FONG

Faculty of Engineering, University of Singapore, Prince Edward Road, Singapore 2, *Republic of Singapore*

(*Received* 30 *July* 1973; *accepted* 16 *November* 1973)

Manual methods employing the Wulff net and stereographic projections are used to determine the crystallographic orientation of hexagonal crystal or grain surfaces from observations of traces of crystallographic planes. Equations are developed which enable such determinations to be carried out easily and precisely with computers for many kinds and combinations of traces observed. A method of this nature should reduce considerably the labour in the single-surface trace analysis of hexagonal crystals or grains.

Introduction

A well-known method of orienting the surface of a crystal or grain is to utilize traces of known crystallographic planes on the surface such as slip lines, twin boundaries, edges of plate-shaped precipitates and etch pits, *etc.* Given traces on the surface of a crystal or grain one may proceed to orient the surface by operating a stereographic plot containing the trace information, a Wulff net, and a standard stereographic plot in the manner described by Barrett (1952) or that described by Reed-Hill & Baldwin (1965). These manual procedures require some amount of labour and practised skill and can be tedious if many orientation determinations are to be made.

More appealing is the analytical or mathematical approach such as that of Tucker & Murphy (1953) for {100} traces on cubic crystals or those of Drazin & Otte (1963) and Fong (1973) developed for {111} traces also for cubic crystals. The attractiveness of this type of approach is that in it are derived equations and mathematical relationships which, although complex for some cases, are readily programmed on a computer so that thereafter the business of obtaining crystal or grain surface orientations from trace observations becomes simply a matter of feeding in trace data to the computer. Precise results are obtained and a multitude of orientation determinations may be performed effortlessly in a short space of time.

In this paper we will develop an analytical or mathematical method of deriving the orientatioo of a hexagonal crystal or grain surface given data on three trace directions on the surface all of $\{h0\bar{h}k\}$ or all of $\{hh\bar{2}\bar{h}k\}$ and usually two other trace directions of any type. It is felt that such a method would be useful as it provides for a labour-saving computerized approach to the problem of orienting the surface of hexagonal crystals, particularly metals, using traces such as twins, slip lines, and basal planes revealed by polarized light.

Preliminary considerations

In Fig. 1 the regular hexagon $A_1A_2A_3A_4A_5A_6$, with centre O, represents the basal plane of a hexagonal crystal. The six planes of $\{h0\bar{h}k\}$ or of $\{hh\bar{2}\bar{h}k\}$ are shown as A_1A_2K, A_2A_3K, A_3A_4K, A_4A_5K, A_5A_6K, and A_6A_1K. We will work in terms of a rectangular coordinate system $OXYZ$ with axis OX parallel to OA_3, axis OY perpendicular to OA_3, and axis OZ in the direction of OK. Thus, in the case of $\{h0\bar{h}k\}$ planes OX, OY, and OZ will be in the directions of $[\bar{1}2\bar{1}0]$, $[\bar{1}010]$, and [0001]; in the case of $\{hh\bar{2}\bar{h}k\}$ planes they will be parallel to $[01\bar{1}0]$, $[\bar{2}110]$, and [0001] respectively. We will also refer to crystallographic directions in terms of vectors referred to the $OXYZ$ system; in the case of planes vectors expressing the directions of their normals will be used. So the six planes A_1A_2K, A_2A_3K, A_3A_4K, A_4A_5K, A_5A_6K, and A_6A_1K are given by $0, 2/\sqrt{3}, g)$,